Observation of Nonlinear Exceptional Points with a Complete Basis in Dynamics

Kai Bai,[1] Tian-Rui Liu,[1] Liang Fang,[1] Jia-Zheng Li,[1] Chen Lin,[1] Duanduan Wan,[1,*] and Meng Xiao[1,2,†]
[1]Key Laboratory of Artificial Micro- and Nano-structures of Ministry of Education and School of Physics and Technology, Wuhan University, Wuhan 430072, China
[2]Wuhan Institute of Quantum Technology, Wuhan 430206, China

(Received 3 July 2023; accepted 12 January 2024; published 16 February 2024)

The exotic physics associated with exceptional points (EPs) is always under the scrutiny of theoretical and experimental science. Recently, considerable effort has been invested in the combination of nonlinearity and non-Hermiticity. The concept of nonlinear EPs (NEPs) has been introduced, which can avoid the loss of completeness of the eigenbasis in dynamics while retaining the key features of linear EPs. Here, we present the first direct experimental demonstration of a NEP based on two non-Hermition coupled circuit resonators combined with a nonlinear saturable gain. At the NEP, the response of the eigenfrequency to perturbations demonstrates a third-order root law and the eigenbasis of the Hamiltonian governing the system dynamics is still complete. Our results bring this counterintuitive aspect of the NEP to light and possibly open new avenues for applications.

DOI: 10.1103/PhysRevLett.132.073802

Introduction.—Non-Hermiticity [1–3] is ubiquitous for a wide variety of classical and quantum systems that exhibit nonconservative phenomena, such as gain, loss, and non-Hermitian couplings [4,5]. Recently, tons of novel phenomena and fascinating potential applications related to exceptional points (EPs) [3,6,7] have revealed that nonconservative elements can drastically alter the behaviors of systems and attract fast-growing efforts [8–32]. At an EP, two or more eigenmodes coalesce and become identical. As a result, the Hamiltonian is defective, and its eigenstates do not span the entire Hilbert space, i.e., the completeness of eigenstates is lost. A defective Hamiltonian leads to a dramatic increase in ubiquitous noise [33–36] and hinders the implementation of EP-related operations. Furthermore, EPs, especially higher-order EPs, require tuning of a considerable number of parameters as they correspond to singularities in a hyperdimensional space [12,37–41], indicating an ultracomplex experimental setup.

In the field of EP sensing, there have been a few ingenious schemes to mitigate the diverging noise associated with the collapse of the eigenmodes and so as to improve the signal-to-noise ratio (SNR) [42–44]. However, the completeness of eigenbasis is still lost. In addition, whether these specific schemes can be extended to other EP-related operations in the presence of noise remains unclear. Clearly, it would be of great interest to pursue a universal approach that can address the increased noise and be extended to more scenarios. Nonlinear EPs (NEPs), unique spectral singularities present in nonlinear non-Hermitian systems, came into being [45,46]. The order of a NEP is determined by the total number of (auxiliary) steady eigenmodes that simultaneously coalesce at that point. Intriguingly, the instantaneous Hamiltonian governing the dynamical evolution of the system can possess a complete eigenbasis. In addition, the key features of conventional linear EPs, such as enhanced responsivity [12,13] and chiral state transfer [16–19], have been retained. The completeness of the eigenbasis is corroborated by a finite Petermann factor (PF) [33–35], instead of a divergent one that typical appear at conventional linear EPs. As a direct consequence, NEPs offer a way out of the dramatically increased noise at linear EPs from its fundamental origin. Meanwhile, compared with a conventional order M EP (EP_M), the number of tuning parameters required to reach an order M NEP (NEP_M) is significantly reduced [47]. It is clear that NEPs are perfectly suitable for detection applications [12,13], metrology and sensing [42,51–54], topological energy transfer [16], polarization states conversion [17], and on-chip optical devices such as optical isolators [20,21], directional lasing [55], etc. Nonetheless, NEPs with a complete basis in dynamics have not yet been demonstrated in any experiment.

Here, designing a minimal scheme combining a non-Hermitian coupling and a nonlinear saturable gain, we demonstrate a NEP_3 whereat the instantaneous Hamiltonian exhibits a complete basis. Our circuit consists of two LC resonators coupled through one capacitor and one resistor, and these two circuit elements together offer a non-Hermitian coupling. One of the resonators is equipped with a saturable gain which consists of a linear voltage amplifier and two diodes. One stable and two auxiliary steady eigenmodes of this circuit coalesce at the NEP_3, and the response of eigenfrequencies demonstrates a third-order root law. Meanwhile, the temporal dynamics of the system are governed entirely by an effective instantaneous Hamiltonian that is anchored by the stable eigenmode.

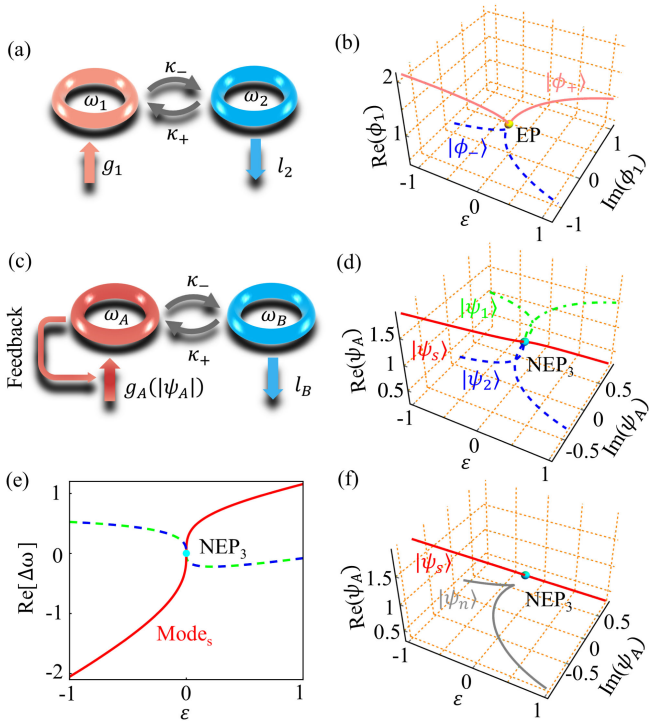

FIG. 1. (a) Schematic of a linear model. It consists of two resonators with resonance frequency $\omega_{1,2}$ and linear gain g_1 and loss l_2. The coupling between them is non-Hermitian. (b) shows the variation of the two eigenstates $|\phi_+\rangle$ and $|\phi_-\rangle$ versus ε. (c) Schematic of our nonlinear model. ψ_A of the three steady states (d) and the real part of corresponding frequency (e) versus ε. (f) shows ψ_A of the two eigenstates of the instantaneous Hamiltonian H_s, which is anchored by the stable eigenmode. The EP and NEP are located at $\varepsilon = 0$. The parameters used are: $\omega_1 = \omega_A = 0$, $\kappa_0 = \kappa_\nu = g_1 = l_2 = 1$, $\omega_2 = 2$, $l_B = 1.14$, and $\omega_B = 1.97$. The specific form of the saturable gain $g_A(|\psi_A|)$ in (c) is irrelevant for the results in (d)–(f) as long as Eq. (5) is satisfied.

Intriguingly, we demonstrate that such an instantaneous Hamiltonian is diagonalizable, thus guaranteeing a complete eigenbasis. The Petermann factor (PF), which is typically used to characterize the nonorthogonality of the eigenbasis, is finite at the NEP$_3$ and thus further verifies our conclusion. Our observations bring the counterintuitive aspect of the NEPs to light and possibly inspire more NEP-related applications in noisy environments.

General theoretical analysis.—We first present a general theoretical analysis to show that a NEP$_3$ with a nondefective instantaneous Hamiltonian is possible with the help of a non-Hermitian coupling. Non-Hermitian couplings have drawn intense interest recently in non-Hermitian systems and led to novel phenomena such as skin effects [5,56], morphing of edge states [57] and etc. [51]. Furthermore, non-Hermitian couplings can also be used to construct conventional linear EPs [58]. The scheme shown in Fig. 1(a) is described by the Hamiltonian near a linear EP is

$$H_l = \begin{pmatrix} \omega_1 + ig_1 & \kappa_+ \\ \kappa_- & \omega_2 - il_2 \end{pmatrix}. \tag{1}$$

Here $\kappa_\pm = \kappa_0 + i\kappa_\nu$, $\kappa_\nu \neq 0$ and $\{\kappa_0, \kappa_\nu\} \in \mathbb{R}$. $\kappa_+ \neq (\kappa_-)^*$ and thus, the coupling is non-Hermitian [58]. In optics, such a non-Hermitian coupling can be introduced with loss or gain elements, and this approach has been demonstrated on different platforms such as optical fibers [59], waveguides [20], and cavities [60]. For simplicity, all the parameters are normalized by κ_0 and an EP is achieved at $\kappa_0 = \kappa_\nu = g_1 = l_2 = 1$, $\omega_2 = 2$, and $\omega_1 = 0$. Let ε represent the external perturbation of one of the system parameters away from those at the EP. Figure 1(b) shows the evolution of the two eigenstates $|\phi_+\rangle$ (pink solid line) and $|\phi_-\rangle$ (blue dashed line) as a function of the external perturbation ε along ω_1, i.e., $\omega_1 + \varepsilon$. Here we only show the fields inside the left resonator, and the fields inside the right resonator are set as 1 for convenience. It is clear that two eigenstates coalesce at $\varepsilon = 0$ where H_l has only one eigenstate $(i, 1)^T$ with the superscript T shorts for transpose. (see Supplemental Material Sec. 1 [61]).

We now turn to consider the nonlinear case as shown in Fig. 1(c). The linear gain above is replaced by a saturable gain $g_A(|\psi_A|)$, which depends on the wave amplitude in resonator A. To distinguish it from the linear system, we use alphabetic subscripts for the nonlinear system. The nonlinear Schrödinger equation is

$$H_{|\boldsymbol{\psi}^R\rangle}|\boldsymbol{\psi}^R\rangle = \omega|\boldsymbol{\psi}^R\rangle, \tag{2}$$

where ω is the eigenfrequency. $|\boldsymbol{\psi}^R\rangle \equiv (\psi_A, \psi_B)^T$ is the right eigenstate, and ψ_A and ψ_B represent the field amplitude of the red (A) and blue (B) resonators, respectively. The nonlinear Hamiltonian is

$$H_{|\boldsymbol{\psi}^R\rangle} = \begin{pmatrix} \omega_A + ig_A(|\psi_A|) & \kappa_+ \\ \kappa_- & \omega_B - il_B \end{pmatrix}. \tag{3}$$

By letting g_A be a free parameter, the eigenfrequency ω of a (auxiliary) steady mode satisfies the cubic function

$$\begin{aligned} p(\omega) &= (\omega - \omega_B)^2(\omega - \omega_A) + l_B^2(\omega - \omega_A) \\ &\quad - 2l\kappa_0\kappa_\nu - (\kappa_0^2 - \kappa_\nu^2)(\omega - \omega_B) \\ &= 0. \end{aligned} \tag{4}$$

Here the corresponding saturated gain value g_s, where a steady state is reached, satisfies

$$-2\kappa_0\kappa_\nu - l_B(\omega_A - \omega) + g_s(\omega_B - \omega) = 0. \tag{5}$$

Note here the specific gain saturation model is irrelevant for $p(\omega)$. To demonstrate the NEP$_3$, we set $\psi_B = 1$ as before, and Figs. 1(d) and 1(e) represent ψ_A and the real part of the eigenfrequency shift $\Delta\omega \equiv \omega - \omega_0$ versus ε imposed on ω_A

(i.e.,$\omega_A + \varepsilon$), respectively. Here, ω_0 is the eigenfrequency of the NEP$_3$ ($\varepsilon = 0$). It is clear that the stable eigenmode (the solid red line) and two auxiliary eigenmodes (green and blue lines) coalesce at the NEP$_3$ [marked by the cyan dot in Figs. 1(d) and 1(e)]. The coalescence of three eigenmodes is the same as that of a PT-symmetrical linear Hamiltonian at an EP$_3$. We emphasize that only the stable mode is physical with a purely real ω, and the other two auxiliary eigenmodes are unphysical as they correspond to complex gain values.

Because of the feedback mechanism of the saturable gain, the nonlinear system will reach a stable state in a short time. Thereafter, the nonlinear gain coefficient $g_A(|\psi_A|)$ is anchored by this stable mode and stays near the corresponding g_s given in Eq. (5). The temporal dynamics are then governed by a 2×2 instantaneous Hamiltonian H_s with $g_A(|\psi_A|)$ in Eq. (3) replaced by g_s. Figure 1(f) shows the evolution of the two eigenstates [$|\psi_s\rangle$ (red line) and $|\psi_n\rangle$ (gray line)] of H_s as a function of ε. Note here, the mode $|\psi_n\rangle$ is not a self-consistent eigenmode of the nonlinear Hamiltonian in Eq. (3). Intriguingly, these two eigenstates do not coalesce at the NEP$_3$ ($\varepsilon = 0$), indicating that the eigenbasis of H_s is complete. Note that a non-Hermitian coupling is necessary for a NEP$_3$ to possess a complete basis in dynamics (see Supplemental Material Sec. 2 [61]). The non-Hermitian coupling in Eq. (3) can be realized with only lossy elements [70,71], and thus the experimental complexity is magnificently reduced. As a consequence, such a minimal tight-binding scheme can be easily implemented in diverse classical and quantum systems [11–13,22–27].

Experimental verification in an electronic circuit.—To observe the aforementioned NEP$_3$, Fig. 2(a) shows a simple and effective circuit with two non-Hermitian-coupled LC resonators we designed [72]. The LC resonator on the right-hand side is lossy with a normal resistor R_B, while the other one possesses an effective negative resistor $-R_A$ that exhibits a saturable gain [42,45,73]. Here, the nonlinear saturation arises from the diodes [42]. (Details provided in Supplemental Material Sec. 4 [61]). Complex voltages V_A and V_B represent the fields inside the corresponding resonators. Assume that the circuit is working with a time-harmonic field $e^{-i\omega t}$, $C_c \ll C_0$ and $|\omega_{A,B} - \omega| \ll \omega$, and use $\omega_{A,B} = 1/\sqrt{L_{A,B}C_0}$ to represent the resonant frequency of the uncoupled resonator, the Kirchoff's equations are

$$\begin{pmatrix} \omega_A + \frac{i}{2C_0}\left(\frac{1}{R_A} - \frac{1}{R_C}\right) & \frac{i}{2C_0R_c} + \omega_B\frac{C_c}{2C_0} \\ \frac{i}{2C_0R_c} + \omega_B\frac{C_c}{2C_0} & \omega_B - \frac{i}{2C_0}\left(\frac{1}{R_B} + \frac{1}{R_C}\right) \end{pmatrix} \begin{pmatrix} V_A \\ V_B \end{pmatrix} = \omega \begin{pmatrix} V_A \\ V_B \end{pmatrix}. \tag{6}$$

Compared with Eq. (3), the coupling, loss, and saturated gain are given by $\kappa_+ = \kappa_- = \omega_B C_c/2C_0 + i/2R_cC_0$, $l_B = 1/2R_cC_0 + 1/2R_BC_0$, and $g_A = 1/2R_AC_0 - 1/2R_cC_0$, respectively. Figure 2(b) shows our experimental setup. As there is an amplifier in the circuit, the system automatically reaches and stays at a stable mode as we tune the dc power supply to provide the operating voltage (± 5 V) of the amplifier. To demonstrate the dynamics from an initial state to the stable state, we applied an external sine driving signal of 1 V and 70 kHz on V_A and waited till the circuit's operating frequency was the same as the driving signal. After that, we remove the external driving signal and start to record the relative waveform as shown in Fig. 2(c). V_A and V_B start oscillation and reach the stable state at around 0.4 ms. Figure 2(d) zooms in this waveform after the stable state is reached, and from this, we can obtain the amplitude, relative phase, and eigenfrequency of the stable mode.

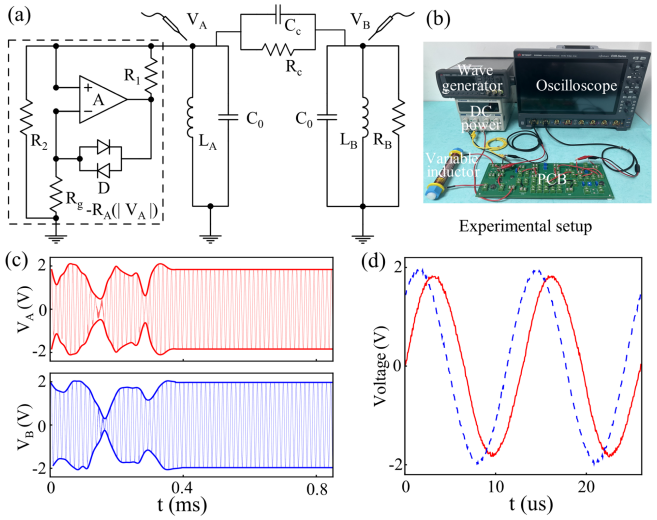

FIG. 2. (a) The circuit used in the experiment, showing the inductors (L), capacitors (C), resistors (R), diodes (D), and an amplifier (A). The black dashed rectangular marks the negative resistor $-R_A(|V_A|)$. (b) A photo of the experimental setup. The oscilloscope records the waveforms of V_A and V_B, which then gives us the corresponding frequencies, voltages, and relative phase. The dc power supplies power for the amplifier, and the arbitrary waveform generator is used to generate the required external driving signal. We add a homemade variable inductor to fine-tune L_A to control the resonance frequency of resonator A [42]. Details of the circuit elements on the printed circuit board (PCB) can be found in Supplemental Material Sec. 5 [61]. (c) Removing the external driving signal of 1 V and 70 kHz, the red and blue lines show the temporal dynamics of V_A and V_B, respectively. At around 0.4 ms, V_A and V_B reach a stable state. The bold red and blue lines highlight the envelope of V_A and V_B, which remain nearly constant after reaching the stable state. (d) Starting at 0.66 ms, zoom in on the dynamics of the stable state. Parameters in the experiments are $L_A = 245.4$ μH, $C_0 = 18.5$ nF, $C_c = 3.9$ nF, $R_c = 760$ Ω, $R_B = 1314$ Ω, and $L_B = 197.7$ μH.

To demonstrate the behavior of the NEP$_3$ in the circuit, we let R_A be a free parameter to solve Eq. (6) and then find the (auxiliary) steady modes. Figures 3(a)–3(c) show the amplitude ratio, relative phase, and the real part of

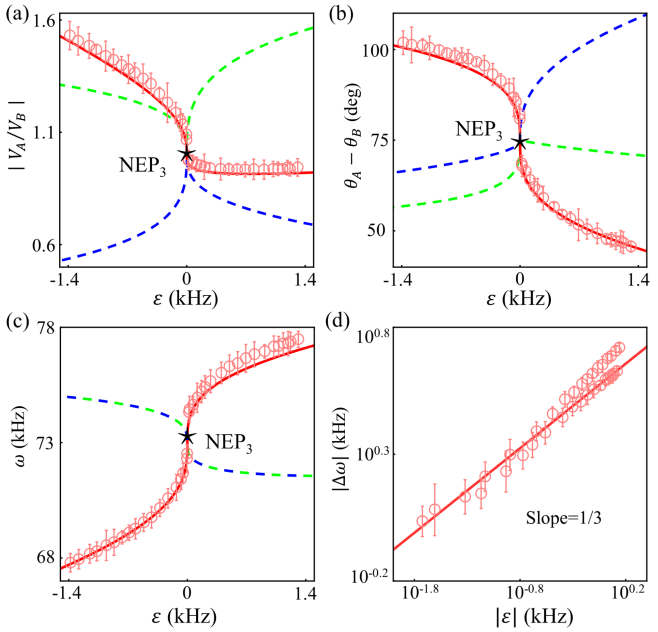

FIG. 3. The voltage amplitude ratio $|V_A/V_B|$ (a), the relative phase $\theta_A - \theta_B$ with $\theta_{A,B} = \arg(V_{A,B})$ (b) and the resonance frequency (c) versus the perturbation ε by varying L_A. Here, the perturbation ε is defined as $\varepsilon \equiv (\omega_A - \omega_{A0})/2\pi$, where ω_{A0} represents the resonance frequency of resonator A when the NEP_3 is reached. (d) The double-log plot of the frequency shift $\Delta\omega = (\omega - \omega_{\mathrm{NEP}_3})/2\pi$ versus the perturbation $|\varepsilon|$, where ω_{NEP_3} represents the eigenfrequency at the NEP_3. The measured values are averaged over 16 independent measurements. The experimental errors (standard deviation) are smaller than the marker size. For demonstration purposes, we exaggerate the error bars in (a)–(d) by factors of 20, 10, 10, and 10, respectively. $L_0 = 253.5$ μH and the other parameters are the same as the Fig. 2.

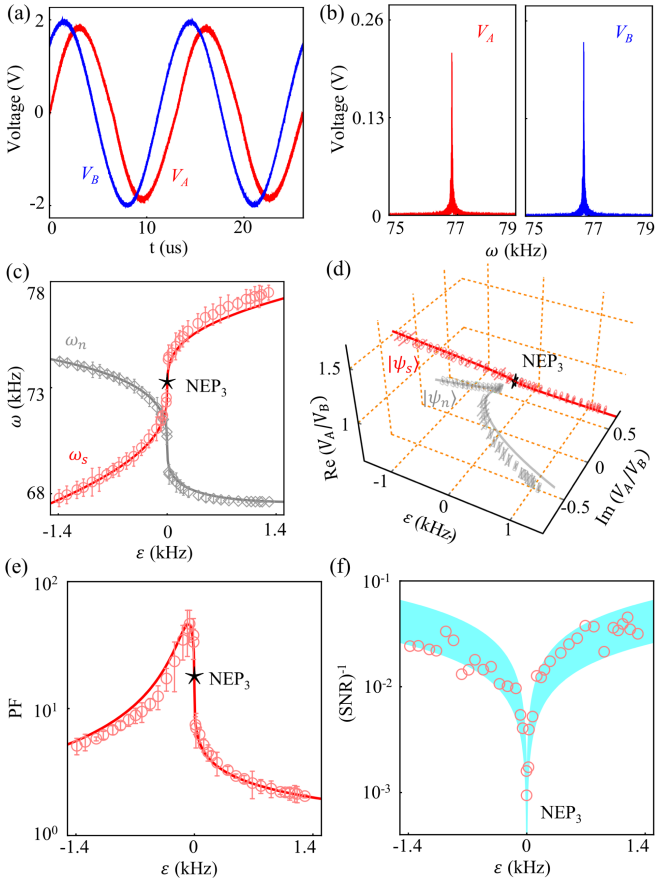

FIG. 4. The dynamics of the stable modes (a) and the corresponding Fourier spectra (b) under an artificial Gaussian noise. The circuit model used is plotted in Fig. S11 [61]. The real part of eigenvalues (c) and V_A/V_B of the eigenstates (d) of H_s, the PF (e), and the SNR (f) versus the external perturbation ε. In (c) and (d), the solid red lines and the dashed gray lines represent the stable and the accompanied eigenmode of H_s. For demonstration purposes, we exaggerate the error bars by a factor of 10, 10, and 15 in (c)–(e), respectively. The cyan area in (f) is for eye guiding. The definition of ε and the parameters used are the same as those in Fig. 3.

eigenfrequencies, respectively. We can see one stable steady eigenmode (red solid lines) and two auxiliary eigenmodes (blue and green dashed lines) coalesce at the NEP_3. In the experiments, only the stable steady eigenstates are reachable, and the measured results (open disks) match perfectly with the simulations. Figure 3(d) shows the frequency shift $\Delta\omega$ versus the perturbation ε on a logarithmic scale. The slope fits well with $1/3$ near the NEP_3 and derivates from $1/3$ when away from the NEP_3. The deviation originates from the parameter dependence of the circuit elements and higher-order corrections. The detailed analysis of experimental error is presented in Supplemental Material Sec. 6 [61].

To clearly see the noisy dynamics after the stable mode is reached, we add an artificial Gaussian noise signal on resonator A with an amplitude of 1 V and a bandwidth of 100 kHz using the arbitrary waveform generator. (Details provided in Supplemental Material Sec. 7 [61]) Compared to Fig. 2(d), the waveform on the oscilloscope exhibits an increased width but only tiny changes in period, voltage ratio, and relative phase [see Fig. 4(a)]. (See the Supplemental Material Sec. 7 [61]) To quantify these changes, Fig. 4(b) shows the corresponding Fourier spectra within the period of $0 < t < 5$ s. Even under such a largely exaggerated amplitude of noise, the change of the frequency and eigenstates, i.e., the amplitude and the relative phase between V_A and V_B are still negligibly small (see Table S1 [61] for more details). Thus, we can conclude that the system is anchored by the stable mode. And, the system's dynamics under noise are governed by the effective instantaneous Hamiltonian H_s with R_A of Eq. (6) replaced by the saturated negative resistance $R_{A,s}$. Figures 4(c) and 4(d) show the real part of the eigenvalues (c) and eigenstates (d) of H_s, where the red line is the same as that in Fig. 3(c), i.e., H_s shares one same eigenmode as the nonlinear system. It is clear that the two eigenmodes of H_s do not coalesce at the NEP_3. Here, the red markers in Figs. 4(c) and 4(d) represent the measured results, and the gray markers are obtained from the

eigensystem of H_s through Eq. (6) with the values of $R_{A,s}$ retrieved from the measurements of the stable mode. And these two eigenvalues ω_s (red markers) and ω_n (gray markers) of H_s in Fig. 4(c) do not intersect because they have different imaginary parts [see Fig. S4(b) [61]]. The PF is a measure of eigenstates' nonorthogonality [33–35]. A finite PF verifies again that the system exhibits a complete basis in dynamics [see Fig. 4(e)]. And SNR, as expected, has been significantly enhanced near the NEP_3 [see Fig. 4(f)]. Moreover, we provide an approach to further reduce the PF at NEP_3 in Supplemental Material Sec. 8 [61].

Conclusions.—In summary, we design a minimal scheme and observe a NEP_3 exhibiting a complete basis in dynamics within an electronic circuit. Compared with traditional circuits to construct a linear EP_3, the number of components used in our circuit is reduced noteworthily. Fewer components indicate a substantial decrease in the experimental complexity; hence, the corresponding system is much more robust. At the NEP_3, the response of the eigenfrequency to perturbations exhibits a third-order root law. Our experiments unambiguously demonstrate the complete basis of an NEP_3 and reveal a significantly enhanced SNR. Illuminating this counterintuitive aspect of NEPs, our findings inspire potential applications in noisy environments and pave the way for introducing NEPs into condensed matter physics and open quantum regimes.

The authors thank Xin Lv, Chong Chen, Chunyin Qiu, and Zhengyou Liu for the helpful discussions. This work is supported by the National Key Research and Development Program of China (Grant No. 2022YFA1404900), the National Natural Science Foundation of China (Grants No. 12274330, No. 12274332, No. 12334015), the China Postdoctoral Science Foundation under Grant No. 2023M742715, the Knowledge Innovation Program of Wuhan-Shuguang (Grant No. 2022010801020125), and the "Xiaomi Young Scholar Program" at Wuhan University.

*ddwan@whu.edu.cn
†phmxiao@whu.edu.cn

[1] W. D. Heiss, J. Phys. A Math. Theor. **45**, 444016 (2012).
[2] I. Rotter, J. Phys. A Math. Theor. **42**, 153001 (2009).
[3] Y. Ashida, Z. Gong, and M. Ueda, Adv. Phys. **69**, 249 (2020).
[4] T. Hofmann, T. Helbig, C. H. Lee, M. Greiter, and R. Thomale, Phys. Rev. Lett. **122**, 247702 (2019).
[5] T. Helbig, T. Hofmann, S. Imhof, M. Abdelghany, T. Kiessling, L. W. Molenkamp, C. H. Lee, A. Szameit, M. Greiter, and R. Thomale, Nat. Phys. **16**, 747 (2020).
[6] M. Berry, Czech. J. Phys. **54**, 1039 (2004).
[7] W. D. Heiss, J. Phys. A **37**, 2455 (2004).
[8] Y. Jiang, Y. Mei, Y. Zuo, Y. Zhai, J. Li, J. Wen, and S. Du, Phys. Rev. Lett. **123**, 193604 (2019).
[9] M. Naghiloo, M. Abbasi, Y. N. Joglekar, and K. W. Murch, Nat. Phys. **15**, 1232 (2019).
[10] L. Ding, K. Shi, Q. Zhang, D. Shen, X. Zhang, and W. Zhang, Phys. Rev. Lett. **126**, 083604 (2021).
[11] W. Tang, X. Jiang, K. Ding, Y.-X. Xiao, Z.-Q. Zhang, C. T. Chan, and G. Ma, Science **370**, 1077 (2020).
[12] H. Hodaei, A. U. Hassan, S. Wittek, H. Garcia-Gracia, R. El-Ganainy, D. N. Christodoulides, and M. Khajavikhan, Nature (London) **548**, 187 (2017).
[13] W. Chen, . Kaya zdemir, G. Zhao, J. Wiersig, and L. Yang, Nature (London) **548**, 192 (2017).
[14] L. Feng, Z. J. Wong, R. M. Ma, Y. Wang, and X. Zhang, Science **346**, 972 (2014).
[15] H. Hodaei, M.-A. Miri, M. Heinrich, D. N. Christodoulides, and M. Khajavikhan, Science **346**, 975 (2014).
[16] H. Xu, D. Mason, L. Jiang, and J. G. E. Harris, Nature (London) **537**, 80 (2016).
[17] A. U. Hassan, B. Zhen, M. Soljačić, M. Khajavikhan, and D. N. Christodoulides, Phys. Rev. Lett. **118**, 093002 (2017).
[18] J. Doppler, A. A. Mailybaev, J. Böhm, U. Kuhl, A. Girschik, F. Libisch, T. J. Milburn, P. Rabl, N. Moiseyev, and S. Rotter, Nature (London) **537**, 76 (2016).
[19] H. Nasari, G. Lopez-Galmiche, H. E. Lopez-Aviles, A. Schumer, A. U. Hassan, Q. Zhong, S. Rotter, P. LiKamWa, D. N. Christodoulides, and M. Khajavikhan, Nature (London) **605**, 256 (2022).
[20] X. L. Zhang, T. Jiang, and C. T. Chan, Light Sci. Appl. **8**, 88 (2019).
[21] Y. Choi, C. Hahn, J. W. Yoon, S. H. Song, and P. Berini, Nat. Commun. **8**, 14154 (2017).
[22] C. Dembowski, H.-D. Gräf, H. L. Harney, A. Heine, W. D. Heiss, H. Rehfeld, and A. Richter, Phys. Rev. Lett. **86**, 787 (2001).
[23] S.-B. Lee, J. Yang, S. Moon, S.-Y. Lee, J.-B. Shim, S. W. Kim, J.-H. Lee, and K. An, Phys. Rev. Lett. **103**, 134101 (2009).
[24] Y. Choi, S. Kang, S. Lim, W. Kim, J.-R. Kim, J.-H. Lee, and K. An, Phys. Rev. Lett. **104**, 153601 (2010).
[25] B. Zhen, C. W. Hsu, Y. Igarashi, L. Lu, I. Kaminer, A. Pick, S.-L. Chua, J. D. Joannopoulos, and M. Soljačić, Nature (London) **525**, 354 (2015).
[26] T. Gao, E. Estrecho, K. Y. Bliokh, T. C. Liew, M. D. Fraser, S. Brodbeck, M. Kamp, C. Schneider, S. Höfling, Y. Yamamoto, F. Nori, Y. S. Kivshar, A. G. Truscott, R. G. Dall, and E. A. Ostrovskaya, Nature (London) **526**, 554 (2015).
[27] A. Regensburger, C. Bersch, M.-A. Miri, G. Onishchukov, D. N. Christodoulides, and U. Peschel, Nature (London) **488**, 167 (2012).
[28] K. Ding, G. Ma, M. Xiao, Z. Q. Zhang, and C. T. Chan, Phys. Rev. X **6**, 021007 (2016).
[29] S. Wang, B. Hou, W. Lu, Y. Chen, Z. Q. Zhang, and C. T. Chan, Nat. Commun. **10**, 832 (2019).
[30] H. Wang, S. Assawaworrarit, and S. Fan, Opt. Lett. **44**, 638 (2019).
[31] S. Assawaworrarit, X. Yu, and S. Fan, Nature (London) **546**, 387 (2017).
[32] C. Liang, Y. Tang, A.-N. Xu, and Y.-C. Liu, Phys. Rev. Lett. **130**, 263601 (2023).
[33] A. E. Siegman, Phys. Rev. A **39**, 1253 (1989).
[34] S.-Y. Lee, J.-W. Ryu, J.-B. Shim, S.-B. Lee, S. W. Kim, and K. An, Phys. Rev. A **78**, 015805 (2008).

[35] H. Wang, Y. H. Lai, Z. Yuan, M. G. Suh, and K. Vahala, Nat. Commun. **11**, 1 (2020).
[36] C. Chen, L. Jin, and R.-B. Liu, New J. Phys. **21**, 083002 (2019).
[37] Z. Lin, A. Pick, M. Lončar, and A. W. Rodriguez, Phys. Rev. Lett. **117**, 107402 (2016).
[38] A. Pick, B. Zhen, O. D. Miller, C. W. Hsu, F. Hernandez, A. W. Rodriguez, M. Soljačić, and S. G. Johnson, Opt. Express **25**, 12325 (2017).
[39] H. Jing, Ş. K. Özdemir, H. Lü, and F. Nori, Sci. Rep. **7**, 3386 (2017).
[40] S. Soleymani, Q. Zhong, M. Mokim, S. Rotter, R. El-Ganainy, and Ş. K. Özdemir, Nat. Commun. **13**, 599 (2022).
[41] X. Zhang, K. Ding, X. Zhou, J. Xu, and D. Jin, Phys. Rev. Lett. **123**, 237202 (2019).
[42] K. Bai, L. Fang, T.-R. Liu, J.-Z. Li, D. Wan, and M. Xiao, Natl. Sci. Rev. **10**, nwac259 (2022).
[43] Z. Li, C. Li, Z. Xiong, G. Xu, Y. R. Wang, X. Tian, X. Yang, Z. Liu, Q. Zeng, R. Lin, Y. Li, J. K. W. Lee, Jason Kai Wei Ho, and C.-W. Qiu, Phys. Rev. Lett. **130**, 227201 (2023).
[44] R. Kononchuk, J. Cai, F. Ellis, R. Thevamaran, and T. Kottos, Nature **607**, 697 (2022).
[45] K. Bai, J.-Z. Li, T.-R. Liu, L. Fang, D. Wan, and M. Xiao, Phys. Rev. Lett. **130**, 266901 (2023).
[46] However, the experimental implementation of such a nonlinear system is challenging [45]. First, though the number of tuning parameters needed is greatly reduced relative to conventional linear EPs, there is still a need to tune five parameters simultaneously. Second, the ultrasensitive parameter dependence at the NEP_5 makes it extremely challenging to approach a NEP_5, especially considering the hyperdimensional parameter space.
[47] Note that, in the absence of any symmetry, order-M EPs generally require the tuning of 2(M-1) real parameters based on counting the freedom of the discriminant [48–50]. However, for most experiments based on coupled resonances, the physical tunable parameters are resonance frequency, gain or loss and the coupling strength. In these cases, the number of tuning parameters are much larger with a minimum number 3(M-1), where the global frequency shift in the complex plane and one parameter for normalization are excluded.
[48] K. Ding, C. Fang, and G. Ma, Nat. Rev. Phys. **4**, 745 (2022).
[49] I. Mandal and E. J. Bergholtz, Phys. Rev. Lett. **127**, 186601 (2021).
[50] S. Sayyad and F. K. Kunst, Phys. Rev. Res. **4**, 023130 (2022).
[51] H.-K. Lau and A. A. Clerk, Nat. Commun. **9**, 4320 (2018).
[52] J. C. Budich and E. J. Bergholtz, Phys. Rev. Lett. **125**, 180403 (2020).
[53] K. Bai, H.-G. Luo, W. Zhang, and M. Xiao, Phys. Rev. A **101**, 022115 (2020).
[54] K. Bai, Z. Peng, H.-G. Luo, and J.-H. An, Phys. Rev. Lett. **123**, 040402 (2019).
[55] B. Peng, K. Özdemir, M. Liertzer, W. Chen, J. Kramer, H. Ylmaz, J. Wiersig, S. Rotter, and L. Yang, Proc. Natl. Acad. Sci. U.S.A. **113**, 6845 (2016).
[56] S. Yao and Z. Wang, Phys. Rev. Lett. **121**, 086803 (2018).
[57] W. Wang, X. Wang, and G. Ma, Nature (London) **608**, 50 (2022).
[58] K. Takata, N. Roberts, A. Shinya, and M. Notomi, Phys. Rev. A **105**, 013523 (2022).
[59] K. Wang, A. Dutt, K. Y. Yang, C. C. Wojcik, J. Vučković, and S. Fan, Science **371**, 1240 (2021).
[60] Z. Gao, X. Qiao, M. Pan, S. Wu, J. Yim, K. Chen, B. Midya, L. Ge, and L. Feng, Phys. Rev. Lett. **130**, 263801 (2023).
[61] See Supplemental Material at http://link.aps.org/supplemental/10.1103/PhysRevLett.132.073802, for (1) conventional linear EP_2 in a two-resonator system; (2) theoretical analysis of the NEP_3; (3) derivation of the arbitrary non-Hermitian coupling in electric circuits; (4) nonlinear saturable gain in our electric circuits; (5) circuit elements on the PCB; (6) experimental error analysis; (7) noisy dynamics of the stable modes; (8) reduce the PF with the aid of INICs. Supplemental Material includes Refs. [4,5,31,42,44,62–69].
[62] B. Zhu, Q. Wang, D. Leykam, H. Xue, Q. J. Wang, and Y. D. Chong, Phys. Rev. Lett. **129**, 013903 (2022).
[63] D. Smirnova, D. Leykam, Y. Chong, and Y. Kivshar, Appl. Phys. Rev. **7**, 021306 (2020).
[64] V. V. Konotop, J. Yang, and D. A. Zezyulin, Rev. Mod. Phys. **88**, 035002 (2016).
[65] Z. Dong, H.-J. Kim, H. Cui, C. Li, C.-W. Qiu, and J. S. Ho, Phys. Rev. Appl. **15**, 024023 (2021).
[66] X. Hao, K. Yin, J. Zou, R. Wang, Y. Huang, X. Ma, and T. Dong, Phys. Rev. Lett. **130**, 077202 (2023).
[67] https://www.ti.com/lit/ds/symlink/lm7171.pdf.
[68] J. D. Cresser, Phys. Rev. A **26**, 398 (1982).
[69] K. J. H. Peters and S. R. K. Rodriguez, Phys. Rev. Lett. **129**, 013901 (2022).
[70] X. Huang and Y.-C. Liu, Phys. Rev. A **107**, 023703 (2023).
[71] X. Huang, C. Lu, C. Liang, H. Tao, and Y. C. Liu, Light Sci. Appl. **10**, 30 (2021).
[72] Generally, the realization of an arbitrary nonreciprocal coupling in a circuit system requires four independently tunable coupling elements, which are a capacitor, a resistor, a negative impedance converter with current inversion (INIC) associated with a capacitor [5] and an INIC associated with a resistor [4] (See Supplemental Material Sec. 3 [61]). The specific nonreciprocal coupling in our setup as shown in Eq. (3) requires only a capacitor C_c and a resistor R_c. This form of nonreciprocal coupling avoids the instability generally involved in INICs.
[73] As outlined by the dashed block in Fig. 2(a), the negative resistor consists of a voltage amplifier A, a series of resistors $\{R_1, R_2, R_g\}$ and a two-diodes D whose resistance R_D is a monotonic decreasing function of the voltage applied on it. $-R_A = -(R_2 R_g R_1/R_D)/(R_2 - R_g R_1/R_D)$ and as a result, the negative resistance is a monotonic decreasing function of V_A.